The Pierre Auger Observatory

P. Bernardini [1 2] C. Bleve[12], G. Cataldi[2], S. D'amico [3 2], I. De Mitri[12], U. Giaccari[12], G. Mancarella[12], G. Marsella [32], D. Martello[12], M.Panareo[32], L.Perrone[32], M. Settimo[12] and the AUGER Collaboration

[1]Dipartimento di Fisica, Università del Salento, Italy

[2]Istituto Nazionale di Fisica Nucleare sez. di Lecce, Italy,

[3]Dipartimento di Ingegneria dell'Innovazione, Università del Salento, Italy

The Pierre Auger Observatory has been conceived to measure the flux, arrival direction distribution and mass composition of cosmic rays from 10^{17} eV to the very highest energies with high statistical significance over the whole sky. To achieve this coverage, the Observatory will have instruments located at two sites, one in each of the Northern and Southern Hemispheres. The astrophysical interest in this energy range is well known, stemming largely from the expectation of spectral features in the decade above 10^{19} eV. In particular, it has been predicted [1,2] that the energy spectrum should steepen sharply above about $6 \times 10^{19} eV$ because of the interaction of primary cosmic rays with the microwave background radiation. There is considerable controversy [3] about the existence, or not, of the predicted steepening, commonly known as the Greisen-Zatsepin-Kuzmin (GZK) cut-off. It is clear, however, that there are cosmic rays with energies well beyond $10^{20} eV$ and major issues are the flux of these events and the accurate measurement of the spectral shape. It is known that the spectrum of cosmic rays extends to at least $3 \times 10^{20} eV$. Above $10^{20} eV$, the rate of events is about $1\ km^2 \times\ sr \times 1\ century$, so that vast areas must be monitored to collect a large statistical sample.

Pierre Auger Observatory has been planned as a pair of arrays. The southern site of the Pierre Auger Observatory covers a total surface of about 3000 km^2 at an altitude of 1400 m near the town of Malargue, in the province of Mendoza, Argentina. The surface detector (SD) is a triangular array of 1600 stations distant 1.5 km from each other. It is overlooked by 24 telescopes arranged in four clusters that altogether make up the fluorescence detector (FD). A layout of the Observatory is presented in Fig. 1.

The water tanks respond to the particle component (mainly muons, electrons and positrons and photons at the distances of importance) and the fluorescence cameras measure the emission from atmospheric nitrogen, which is excited by the charged particles of the shower as they traverse the atmosphere. Both techniques, already used for many years to study extensive air showers [4,5], are brought together in a *hybrid* detector to observe showers simultaneously with different techniques.

The surface array will have the following properties:

- 100% duty cycle.
- A well-defined aperture that is independent of energy above 10^{19} eV.
- Uniform coverage in right ascension on a daily basis.
- A response that is largely independent of weather conditions.
- The quality of the data for each event improves with energy.
- Sensitivity to showers arriving at large zenith angles.
- In situ calibration of the detectors by cosmic ray muons.
- Measurement of the time structure of the arriving signals, which is sensitive to the mass of the primary particles.

The fluorescence detectors can be operated during clear nights with little moonlight and have the following characteristics:

- Every event above 10^{19} eV is registered by at least one fluorescence detector: 60% of these events will be recorded by two or more fluorescence detectors. Essentially, every trans-GZK event will be a stereo event. Multiple station coverage improves the energy resolution.
- The longitudinal development profile is measured directly.
- The fluorescence detectors provide a more direct measure of the shower energy. The small, unseen, fraction of the total energy

carried by neutrinos and muons depends somewhat on the mass of the primary particle as well as on the hadronic interaction model.

In this review only the contribution by the Lecce group will be reported.

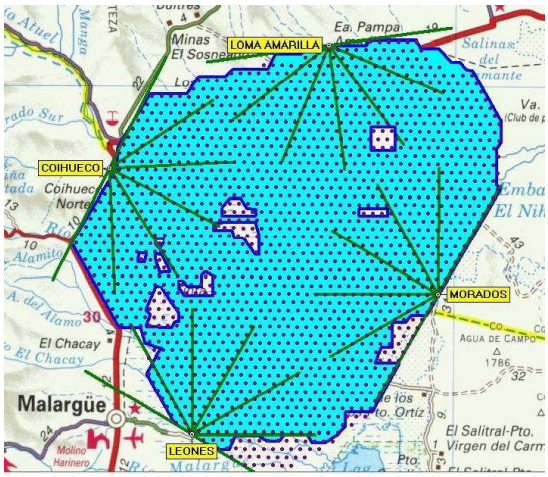

Figure 1. Layout and status of the Pierre Auger Southern Observatory. Each dot marks the position of one SD station; the shaded (blue) area covers the stations active. The 4 FD sites are labeled in yellow, with the field of view of each telescope (6 per site) indicated by green lines (whose length, to illustrate the scale, corresponds to 20 km

Hybrid angular resolution with Corsika showers A precise knowledge of arrival direction of observed events is required for the study of cosmic rays sources. Here the angular resolution (AR) for the hybrid detector of the Pierre Auger Observatory is derived using Corsika [6] showers and a full detector simulation. For the surface detector (SD) events the angular resolution is determined following the time variance model described in [7].

In the hybrid mode, the combination of SD and FD information assures a precise knowledge of the arrival direction down to lower energies. The resolution of arrival direction has been investigated by computing the space angle between injected and reconstructed axes. The simulation sample consists of about 6000 proton Corsika showers with zenith angle distributed as $\sin\theta\cos\theta$ (θ <65°) and energies ranging between 10^{17} and 10^{19} eV in steps of 0.25 in logarithmic scale. A detailed simulation [8] is performed to take into account the hybrid detector response. In order to maximize the usage of the Corsika showers, each shower has been used 5 times, each time with a different core position in order to increase the statistics with a negligible degree of correlation. The layout used for simulations consists of an ideal array of active stations with 24 telescopes in acquisition.

Events with a good geometry reconstruction and with wide (larger than 15°) angular tracks observed in fluorescence telescopes are selected. The angular resolution for hybrid events is defined as the angle corresponding to the 68% of the cumulative distribution function of the space angle between reconstructed an true axes. Figure 2 shows the hybrid angular resolution as a function of energy. At energy larger than $10^{17.5}$ eV the angular resolution is less than 1 degree and at energy above $10^{18.5}$ is about 0.5 degrees. This result doesn't change when performing time dependent simulations which reproduce the realistic atmospheric conditions and the actual hybrid detector configurations.

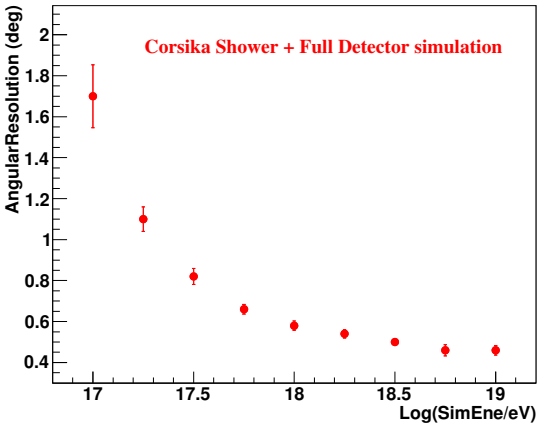

Figure 2. Hybrid angular resolution as a function of the true energy

Spectrum from hybrid data In this analysis, the energy spectrum of cosmic rays is measured using hybrid data collected between December 2004 and February 2007 [9]. The inspected energy range covers a region where the transition from Galactic to extra-galactic cosmic rays is expected to occur.

Due to construction, the configuration of fluorescence telescopes and surface detector has evolved significantly and the effective detection area has correspondingly changed. The key points of the analysis are an accurate estimate of the hybrid

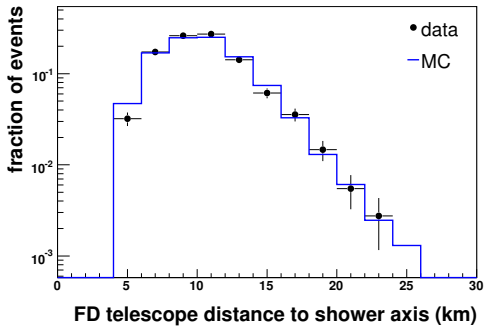

Figure 3. Distribution of telescope distance to shower axis, for data and simulation (same selection cuts applied).

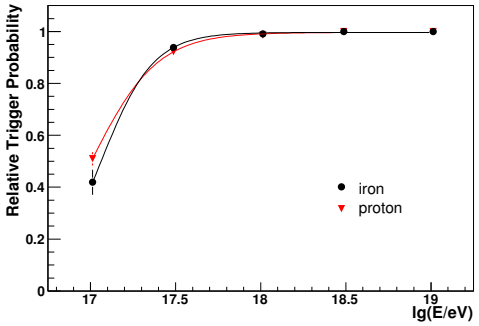

Figure 4. Hybrid trigger efficiency for proton and iron (full simulation method)

detector exposure and an appropriate selection of well-reconstructed events. A good knowledge of systematic uncertainties is also required to support the robustness of the results. The calculation of the hybrid exposure relies on a detailed simulation of fluorescence (FD) and surface detector (SD) response. To reproduce the exact working conditions of the experiment and the entire sequence of given configurations, a large sample of Monte Carlo simulations have been performed. Several factors (fast growth of surface array and ongoing extension of the fluorescence detector, seasonal and instrumental effects) can introduce a significant dependence of aperture on time. This effect has been taken into account and simulated using an accurate calculation of the hybrid detector uptime. The simulation sample consists of a large number of longitudinal energy deposit profiles generated with CONEX [11]. The energy spectrum ranges from 10^{17}eV to 10^{21}eV according to a power-law function with differential spectral index -2 (reweighted to -2.8 when comparing data to simulation) and the zenith angles are sampled between 0° and 70°. The simulation has been validated by comparing the distribution of reconstructed observables to experimental data. Fig. 3 shows the distribution of the telescope distance to shower axis, for data and simulation. A very good agreement is found at this selection level.
The distribution of particles at ground is not provided by CONEX. Nevertheless, the time of the station with the highest signal is sufficient information for this analysis. This time is used in the hybrid reconstruction for determining the incoming direction of the showers, and the impact point at ground. Once the shower geometry is known, the longitudinal profile can be reconstructed and the energy calculated. The tank trigger simulation is performed using a parameterisation based on "Lateral Trigger Probability" functions (LTPs) [12]. They give the probability for a shower to trigger a tank as a function of primary cosmic ray energy, mass, direction and tank distance to shower axis. A full hybrid simulation with CORSIKA showers [6] (FD and SD response are simultaneously and fully simulated) has shown that the hybrid trigger efficiency (a fluorescence event in coincidence with at least one tank) is flat and equal to 1 at energies greater than 10^{18} eV. This feature is shown in Fig. 4 for proton and iron primaries. For these energies, the hybrid trigger efficiency coincides with the one derived from the LTPs based method. The difference between the two primaries becomes negligible at energy larger than $10^{17.5}$ eV. A detailed description of the hybrid detector simulation program is given in [8]. Only data with a successful hybrid geometry reconstruction are selected for calculating the hybrid spectrum. To suppress monocular events with random surface detector triggers, only events with the station used for reconstruction lying within 750 m from the shower axis are accepted. This condition ensures that the probability of the station to trigger is equal to one. Showers that are expected to develop outside the geometrical field of view of the fluorescence detectors are also rejected and, based on data, a fiducial volume for detection is defined as a function of the reconstructed energy. Details on how the fiducial volume is taken are given in [13]. Moreover, only events with reconstructed zenith angle less than 60° are accepted. The observed profile and reconstructed shower depth at maximum (X_{max}) are required to satisfy the following conditions:
- a successful Gaisser-Hillas fit with χ^2/Ndof $<$ 2.5 for the reconstructed longitudinal profile
- minimum observed depth $< X_{max} <$ maximum observed depth
- a relative amount of Cherenkov light in the sig-

nal less than 50%
- measurement of atmospheric parameters available.
A fluorescence photon yield according to [14] is currently used for energy reconstruction. Finally, as the algorithm used for the profile reconstruction propagates both, light flux and geometrical uncertainties, the estimated uncertainties of shower energy is a good variable to reject poorly reconstructed showers. We require $\sigma(E)/E < 20\%$. Fig. 5 shows the hybrid exposure (top) and the energy distribution of all events (bottom) at the last reconstruction level (all quality cuts have been applied). Exposure at this level depends very weakly on chemical composition, giving a spectrum basically independent of any assumption on primaries mass. The hybrid

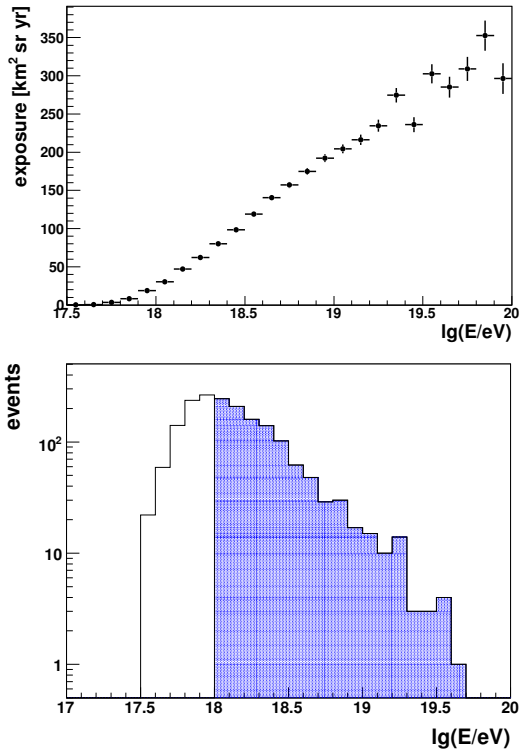

Figure 5. Hybrid exposure after all cuts (top). Energy distribution of selected data (bottom). The number of events used for the spectrum (E $> 10^{18}$ eV, shadowed area) is 1092.

spectrum deriving from this analysis is shown in Fig. 6 compared with the spectrum from surface detector presented in [16] (only statistical uncertainties are given in the figure).
The hybrid spectrum is primarily affected by the systematic uncertainty on the energy determination (about 22% [10]). The calculation of detector

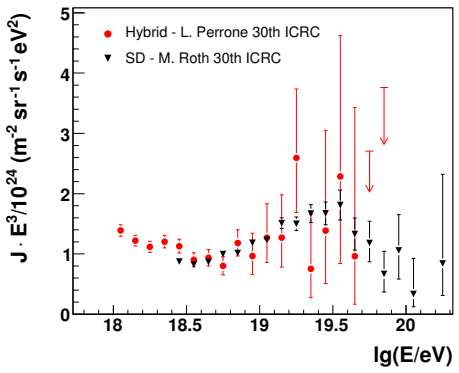

Figure 6. Hybrid energy spectrum shown in comparison with surface detector spectrum (only statistical uncertainties are given in the figure).

uptime has been independently cross-checked using the observed laser shots fired by the Central Laser Facility (CLF) [15] and the results agree at the level of 4%. A more significant source of uncertainty (16 %) is expected from the lack of a precise knowledge of atmospheric conditions. Part of the shower profile may be shadowed by clouds or the Cherenkov light can be diffused by fog and/or clouds and redirected towards the detector. This uncertainty is still large but it is expected to be significantly reduced when all atmospheric monitoring data have been fully analysed. As a final remark, it is worth saying that the extension to the viewing elevations of FD telescopes will allow to be reached lower energies with smaller systematics [17].

Spectrum from Surface Detector data

A set of well reconstructed hybrid data (661 hybrid events collected in the time window between 1/1/2004 and 31/7/2007) have been used to calibrate the surface detector energy estimator S_{38°. S_{38° is the particle density at ground taken at 1000 m from shower axis if the event would had arrived with zenith angle of 38°. This calibration procedure has been designed to maximize the benefits of the surface detector (100% duty cycle and large number of events) and the fluorescence detector (quasi-unbiased calorimetric energy measurement). Fig. 7 shows the correlation of S_{38° with the energy provided by the fluorescence detectro E_{FD}. The calibration is then applied to the entire data set collected by the surface detector (about 20.000 events) and a spectrum is calculated using a SD-based geometric aperture of about 7000 km^{2}sr y. Details of the analysis are given in [18]. It's worthwhile reminding that the aperture used for this analysis doesn't depend on simulations since only events with 100% trigger-

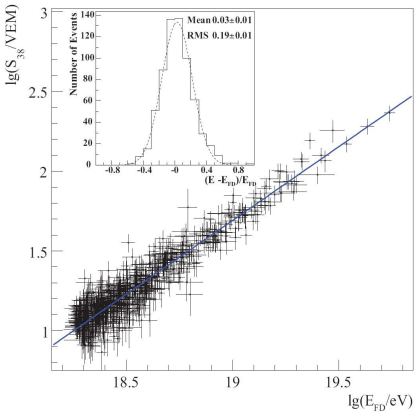

Figure 7. Correlation between $\lg S_{38^\circ}$ and $\lg E_{FD}$ for the 661 hybrid events used in the fit.

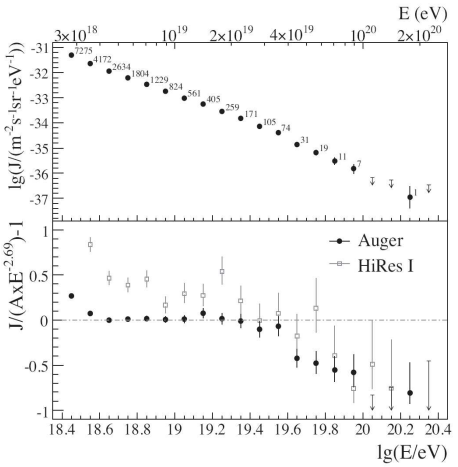

Figure 8. Upper panel: The differential flux from the surface detector as a function of energy. Lower panel: The fractional differences between Auger and Hires I data.

ing probability (E> $10^{18.5}$) are accepted. The energy spectrum shown in Fig.8 is fitted by a smooth transition function. A method which is independent of the slope of the energy spectrum is used to reject a single power-law hypothesis and a flux suppression is observed for E > 4 10^{19} eV with a significance of more than 6 standard deviations. The fractional differences between Auger and Hires I data are also shown in Fig.8. An energy shift of about 15% would result in a very good agreement between the two experiments. Given that, the current estimated uncertainty on the energy scale is about 22% (dominated by the uncertainty on the fluorescence yield), results are compatible within their uncertainties.

Upper limit on the cosmic-ray photon fraction at EeV energies from the Pierre Auger Observatory

Data taken at the Pierre Auger Observatory were searched previously for ultra-high energy (UHE) photons above 10 EeV [20,21]. In Ref. [20], the depth of shower maximum $X_{\rm max}$ of air showers observed by fluorescence telescopes in hybrid mode (i.e. with additional timing information from the ground array) was used to place an upper limit of 16% on the photon fraction above 10 EeV, confirming and improving on previous limits from ground arrays [22–25]. In Ref. [21], the larger number of events taken with the Auger ground array alone allowed us to place a limit of 2% above 10 EeV, which imposes severe constraints on "top-down" models for the origin of ultra-high energy cosmic rays.

Observations in hybrid mode are also possible at energies below 10 EeV. Decreasing the energy threshold increases the event statistics, which to some extent balances the factor ∼10 smaller duty cycle compared to observations with the ground array alone. Thus, based on the previous work, the search for photons is extended to lower energy (here down to 2 EeV).

Photons at EeV energies are expected to be produced in our cosmological neighborhood, as the energy attenuation length of such photons is only of the order of a few Mpc. Possible sources of EeV photons are the standard GZK process (see e.g. Refs. [26–28]), the production by nuclei in regions of intense star light (e.g. in the galactic center [29]), or exotic scenarios such as top-down models (see Ref. [30] for a review). Compared to our previous constraints on top-down models from Ref. [21], the bounds derived in this analysis provide a test of model predictions in a different energy range and using a different experimental technique, thus giving an independent confirmation of the model constraints.

Limits on EeV photons reduce corresponding systematic uncertainties in other analyses of air shower data. For instance, the presence of a substantial photon component can severely affect the reconstruction of the energy spectrum [31], the derivation of the proton-air cross-section [32,33], and the interpretation of the observed average $X_{\rm max}$ [34] in terms of a nuclear primary composition. All details of the analysis are presented in[35]. Here some of the basic tools used to derive the upper limit will be reviewd. A key paratemeter for the determination of an upper limit is the estimate of the detector acceptance. To evaluate the detector acceptance as a function

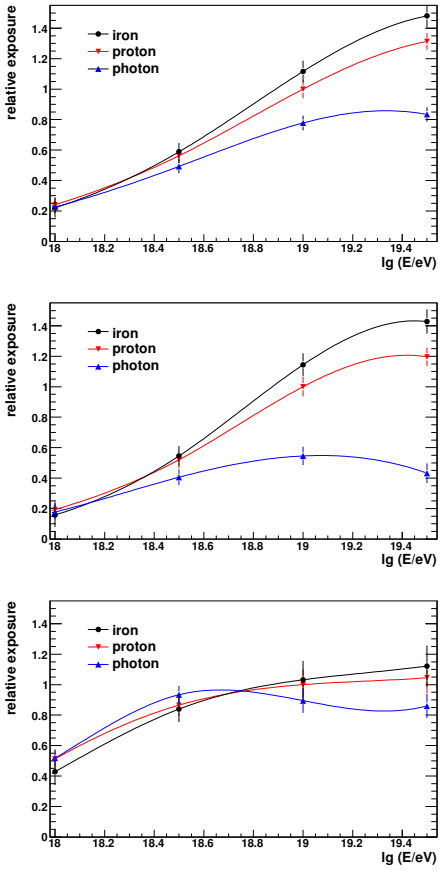

Figure 9. Relative exposure to primary photons, protons and iron nuclei, normalized to protons at 10 EeV. Top panel requiring hybrid trigger, center panel after applying quality cuts, bottom panel after applying fiducial volume cuts (see text). In order to guide the eye polynomial fits are superimposed to the obtained values.

of energy for different primary particles, simulations have been performed using CORSIKA [6] with QGSJET01 [36] and FLUKA [37] as high- and low-energy hadronic interaction models respectively. The Monte Carlo showers have been processed through a complete detector simulation and reconstruction chain [8,38]. In Fig. 9 we show the energy-dependent relative exposure obtained after trigger, quality cuts (well reconstructed events), and fiducial volume cuts (shower maximum observable for any primary type) for primary photons, protons and iron nuclei (normalized to 10 EeV protons). After fiducial volume cuts, the acceptance for photons is close to the acceptance for nuclear primaries.

We therefore adopt for our analysis the method applied in Ref. [21] which needs as an input the total number of events, the number of photon candidates (events having "photon-like" characteristics) and proper correction factors accounting for inefficiencies. The 95% c.l. upper limit $F_\gamma^{95}(E_{\rm thr})$ on the fraction of photons in the cosmic-ray flux above $E_{\rm thr}$ is then given by

$$F_\gamma^{95}(E_{\rm thr}) = \frac{n^{95}_{\gamma-{\rm cand}}(E^\gamma_{\rm thr})}{n_{\rm total}(E^\gamma_{\rm thr})} \ , \qquad (1)$$

where $n^{95}_{\gamma-{\rm cand}}$ is the 95% c.l. upper limit on the number of photon candidates and $n_{\rm total}$ the total number of selected events.

The upper limit on the number of photon candidates $n^{95}_{\gamma-{\rm cand}}$ is given by $n^{95}_{\gamma-{\rm cand}} = n^{95}_{\gamma-{\rm cand,obs}}/\epsilon_{\rm obs}$, where $n^{95}_{\gamma-{\rm cand,obs}}$ is the 95% c.l. upper limit on the number of photon candidates $n_{\gamma-{\rm cand,obs}}$ extracted ("observed") from the data set and $\epsilon_{\rm obs}$ is the corresponding efficiency. $n_{\gamma-{\rm cand,obs}}$ is taken as the number of events which have the observed $X_{\rm max}$ above the median $X^{\gamma,{\rm med}}_{\rm max}$ of the distribution expected for photons of that energy and direction ("photon candidate cut") and that pass the individual cloud check.

There are $n_{\gamma-{\rm cand,obs}} = 8,\ 1,\ 0,\ 0$ photon candidate events with energies greater than 2, 3, 5 and 10 EeV, respectively.

We checked with simulations whether the observed number of photon candidate events is significantly larger than the expectation in case of nuclear primaries only, i.e. whether primary photons appear to be required to explain the photon candidates. The quantitative estimation of the background expected from nuclear primaries suffers from substantial uncertainties, namely the uncertainty of the primary composition in this energy range (a larger background to photons would originate from lighter nuclear primaries) and the uncertainty in the high-energy hadronic interactions models (for instance, reducing the proton-air cross-section allows proton primaries to penetrate deeper into the atmosphere). From simulations using QGSJET01 as the hadronic interaction model, we found that the observed number of photon candidate events is well within the number of background events expected from a pure proton and a pure iron composition. For energies larger than 2 EeV about 30 events are expected in the analyzed time window for proton and 0.3 for iron. The corresponding numbers above 3, 5, 10 EeV are about 12, 4, 1 events for proton and about 0.2, 0.1, 0.0 events for iron. Scenarios of a mixed composition, as also favored by our results on $<X_{\rm max}>$ [34], can reproduce the observation. We conclude that the observed photon candidate events may well be due to nuclear primaries only.

Applied to the data, upper limits of 3.8%, 2.4%, 3.5% and 11.7% on the fraction of cosmic-ray photons above 2, 3, 5 and 10 EeV are obtained at 95% c.l..

The derived upper limits are shown in Fig. 10

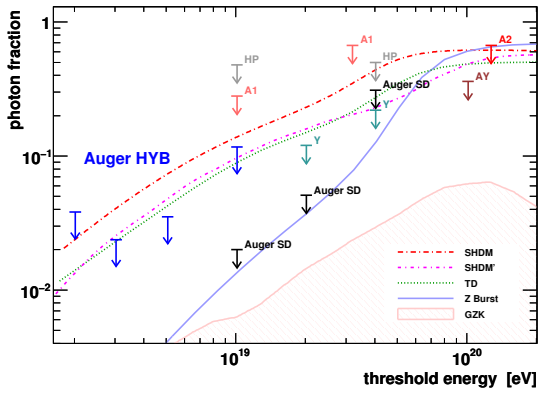

Figure 10. Upper limits on the photon fraction in the integral cosmic-ray flux for different experiments: AGASA (A1, A2) [22,23], AGASA-Yakutsk (AY) [42], Yakutsk (Y) [43], Haverah Park (HP) [24,25]. In black the limits from the Auger surface detector (Auger SD) [21] and in blue the limits above 2, 3, 5, and 10 EeV derived in this work (Auger HYB). The shaded region shows the expected GZK photon fraction as derived in [26]. Lines indicate predictions from top-down models, see [27,44] and [39].

along with previous experimental limits and model predictions (see Ref. [39] for a review and references). These new bounds are the first ones at energies below 10 EeV and, together with *Hybrid-1*, the only ones obtained so far from fluorescence observations (all other limits coming from ground arrays). The results confirm the previous constraints on top-down models from Auger surface detector data. It should be noted that due to the steep flux spectrum, even the previous Auger bound of 2% above 10 EeV only marginally constrains the photon contribution above lower threshold energies (for instance, even above 5 EeV, $\sim$75% of the events are in the previously untested energy range of 5$-$10 EeV).

REFERENCES

1. Greisen, K., Phys Rev Letters, 16 (1966) 748.
2. Zatsepin, G.T. and Kuzmin, V.A., Sov. Phys. JETP Letters, 4 (1966) 78.
3. Takeda, M.*et al.*, Astropart. Phys., 19 (2003) 447.
4. Lawrence, M.A., Reid, R.J.O. and Watson, A.A., J Phys G, 17 (1991) 733
5. Baltrusaitas, R.M. *et al.*, NIM, A240 (1985) 410.
6. D. Heck *et al*, Report FZKA 6019, (1998).
7. C. Bonifazi [Pierre Auger Collaboration], 29th International Cosmic Ray Conference (ICRC 05), Pune, India (3-10 August 2005),
8. S. Argirò *et al.*, NIM A580, (2007), 1485.
9. L. Perrone [Pierre Auger Collaboration], 30th International Cosmic Ray Conference (ICRC 07), Mérida, Yucatan, Mexico (3-11 July 2007),
10. B. Dawson [Pierre Auger Collaboration], 30th International Cosmic Ray Conference (ICRC 07), Mérida, Yucatan, Mexico (3-11 July 2007),
11. T. Bergmann *et al* Astropart. Phys. 26, (2007) 420.
12. E. Parizot [Pierre Auger Collaboration] 29th International Cosmic Ray Conference (ICRC 05), Pune, India (3-10 August 2005),7, (2005) 71-74.
13. Pierre Auger Collaboration [J. Abraham *et al.*], Astropart. Phys., 27 (2007) 155.
14. M. Nagano *et al* Astropart. Phys. 22 (2004) 235.
15. S. BenZvi [Pierre Auger Collaboration] 30th International Cosmic Ray Conference (ICRC 07), Mérida, Yucatan, Mexico (3-11 July 2007),
16. M. Roth [Pierre Auger Collaboration] 30th International Cosmic Ray Conference (ICRC 07), Mérida, Yucatan, Mexico (3-11 July 2007),
17. H. Klages [Pierre Auger Collaboration] 30th International Cosmic Ray Conference (ICRC 07), Mérida, Yucatan, Mexico (3-11 July 2007),
18. Pierre Auger Collaboration [J. Abraham *et al.*], Phys. Rev Lett., 101 (2008) 061101
19. R.U.Abbasi et al, Phys. Rev. Lett., 100 (2008) 101101
20. Pierre Auger Collaboration [J. Abraham *et al.*], Astropart. Phys., 27 (2007), 155.
21. Pierre Auger Collaboration [J. Abraham *et al.*], Astropart. Phys., 29 (2008), 243.
22. K. Shinozaki *et al.*, Astrophys. J., 571 (2002) L117–L120.
23. M. Risse *et al.*, Phys. Rev. Lett., 95 (2005), 171102.
24. M. Ave, J. A. Hinton, R. A. Vazquez, A. A. Watson, and E. Zas, Phys. Rev. Lett., 85 (2000), 2244.
25. M. Ave, J. A. Hinton, R. A. Vazquez, A. A. Watson, and E. Zas, Phys. Rev. D, 65 (2002), 063007.
26. G. Gelmini, O. Kalashev, and D. V. Semikoz, JCAP, 11 (2007).
27. G. Gelmini, O. Kalashev, and D. V. Semikoz, `(astro-ph/0506128)`.
28. G. Sigl, Phys. Rev. D, 75 (2007), 103001.
29. A. Kusenko, J. Schissel, and F. W. Stecker, Astropart. Phys., 25 (2006), 242–245.
30. P. Bhattacharjee and G. Sigl, Phys. Rep., 327

(2000), 109–247.
31. N. Busca, D. Hooper, and E. W. Kolb, Phys. Rev. D, 73(2006), 123001.
32. K. Belov [HiRes Collaboration], Nucl. Phys. B Proc. Suppl., 151 (2006), 197.
33. R. Ulrich, J. Blümer, R. Engel, F. Schüssler, and M. Unger, Nucl. Phys. B Proc. Suppl., 175 (2008), 121,
34. M. Unger [Pierre Auger Collaboration], 30th International Cosmic Ray Conference (ICRC 07), Mérida, Yucatan, Mexico (3-11 July 2007),4 (2007), 373.
35. Pierre Auger Collaboration [J. Abraham *et al.*], "Upper limit on the cosmic-ray photon fraction at EeV energies from the Pierre Auger Observatory", `(arxiv.org/pdf/0903.1127v1`
36. N. N. Kalmykov and S. S. Ostapchenko, Phys. of At. Nucl., 56 (1993), 346–353.
37. A. Fassò, A. Ferrari, J. Ranft, and B. E. Sala, *CERN-2005-10, INFN/TC_05/11, SLAC-R-773*.
38. L. Prado Jr. *et al.*, Nucl. Instr. Meth., A 545 (2005), 632–642.
39. M. Risse and P. Homola, Mod. Phys. Lett. A, 22 (2007), 749.
40. Pierre Auger Collaboration [J. Abraham *et al.*], Phys. Rev. Lett., 101 (2008), 061101.
41. M. Risse *et al.*, Czech. J. Phys. A, 56 (2006), 327.
42. G. Rubtsov *et al.*, Phys. Rev. D, 73 (2006), 063009.
43. A. V. Glushkov *et al.*, JETP Lett., 85 (2007), 163..
44. J. Ellis, V. E. Mayes, and D. V. Nanopoulos, Phys. Rev. D, 74 (2006), 115003.